Contents lists available at ScienceDirect

European Polymer Journal

A wound dressing based on a track-etched membrane modified by a biopolymer nanoframe: physicochemical and biological characteristics

Pavel A. Markov [a,*], Iliya I. Vinogradov [b], Elena Kostromina [a], Petr S. Eremin [a], Ilmira R. Gilmutdinova [a], Irina S. Kudryashova [a], Anastasiya Greben [a], Andrey P. Rachin [a], Alexandr N. Nechaev [b]

[a] *National Medical Research Center of Rehabilitation and Balneology, Moscow 121099, Russian Federation*
[b] *Joint Institute for Nuclear Research, Dubna 141980, Russian Federation*

ARTICLE INFO

ABSTRACT

Ion track membranes (TMs) are obtained by irradiating thin polymer films, which are usually composed of polycarbonate and polyethylene terephthalate (PET). In medicine and biology, TMs are used for the filtration and separation of molecules and cells in addition to studies of cell migration, intercellular interactions, cell proliferation, and differentiation processes. However, the possibilities and prospects of using TMs as components of wound dressings have not been sufficiently explored. In our study, TMs composed of PET were tested since this material is biocompatible and used in prosthetics and reconstructive surgery. The method of combining TM and electroforming nanofibers, which we used in this study, is relatively new and still requires additional research.

Thus, it was found that the main structural elements of the TM surface covered with a biolayer of a mixture of collagen and chitosan are fibers. Coating the TM with a bio-layer preserves its gas and water permeabilities. By varying the fixation method of the biopolymer layer, it is possible to regulate the physicochemical and biological functional properties of the wound dressing. The combination of the high biocompatibility of natural polymers and the stability of synthetic materials can be a successful strategy in manufacturing wound dressings of a new type with specified functional properties. Ion-track PET membranes with applied electrospun fibers from a mixture of chitosan and collagen can be used to produce the wound dressing.

Abbreviated title: A wound dressing based on a track-etched membrane.

1. Introduction

Damage to the skin resulting from mechanical, physical, and/or chemical factors in addition to chronic wounds can cause complications ranging from severe to lethal [1]. To improve the effectiveness of treatment, new treatment technologies are under investigation, including the use of wound dressings with specified functional properties. These properties include hypoallergenic, absence of toxic and local irritating effects, atraumatic when used and replaced, capability of maintaining the microenvironment (pH, humidity, temperature), protection from exogenous infections, and others [2–4]. The technology of developing new composite membrane materials based on an ion track membrane (TM) and a nano-frame made of biopolymers (chitosan, collagen, hyaluronic acid, etc.) can become an innovative approach in the design of a new type of wound dressings [5].

TMs are obtained by irradiating thin polymer films, usually composed of polycarbonate and polyethylene terephthalate (PET), with fast heavy ions followed by photosensitization and chemical etching. A traditional application of TM is laboratory filtration. TM is considered a very good instrument when small particles should be collected onto the membrane surface and analyzed [6,7]. In medicine and biology, TMs are used for the filtration and separation of molecules and cells in addition to studies of cell migration, intercellular interactions, cell proliferation, and differentiation processes [8–11]. However, the possibilities and prospects of using TM as a component of wound dressings have not been sufficiently explored. In the meantime, the presence of micropores in combination with the TM plasticity can protect against invasion of exogenous microflora and both gas and water permeability and is atraumatic when applying a TM-based wound dressing.

In the meantime, the presence of micropores in combination with the

---

TM plasticity can protect against invasion of exogenous microflora, provide both gas and water permeability and is atraumatic when applying a TM-based wound dressing.

In our study, TM composed of PET was tested since this material is biocompatible and is used in prosthetics and reconstructive surgery [12,13]. To impart new functional properties, such as cytocompatibility, regulated cell adhesion, controlled release of biologically active substances, and others, to TM, the method of electroforming a bio-layer of chitosan and collagen on the surface of TM was used. Chitosan is a natural polymer obtained from the partial deacetylation of crustacean waste and possesses anti-algal, anti-fungal, and anti-microbial properties. Moreover, chitosan can substantially support cell adhesion and proliferation [14–16] Collagen, which is the most common protein of the intercellular matrix, is used to give plasticity to biomaterials and at the same time has low immunogenicity and good biocompatibility [17,18].

The electroforming method is well known and is used for making tissue-engineered constructs. The advantage of this method is facilitation of the regulation of the physical, chemical, and biological properties of nanofibers [19,20]. However, the method of combining TM and electroforming nanofibers is relatively new [21] and still requires additional research. For example, various chemical and physical methods are used to impart mechanical stability to electrospun fibers [19,22,23]. However, it is still unknown how the stabilization process affects the structural and functional properties of the composite material. In this study, two methods of stabilizing the bio-layer were used and compared: 1) chemical, using glutaraldehyde (GA) vapors, and 2) thermal, by heating the biomaterial in a furnace.

Thus, the study aimed to characterize the effects of chemical and thermal methods of stabilizing the bio-layer on the physicochemical properties, biodegradation, and biocompatibility of a wound covering based on PET ion track-etched membranes.

2. Materials and methods

Materials and methods.

2.1. Reagents

Several reagents were used in this study: PET (Hostaphan® RNK, Mitsubishi Polyester Film GmbH, Germany); commercial chitosan (Mw 200,000, degree of deacetylation 80–85%; Bioprogress, RF); (3) commercial type I collagen, hydrolyzed from bovine skin (MOBITEK-M, RF). Polyethylene oxide (Mw 300,000), GA solution grade II 25% w/v, PKH-29 and bovine serum albumin (BSA) were obtained from Sigma-Aldrich (Germany). Glacial acetic acid (CH3COOH, Mw 60.05, greater than 99%) was purchased from AppliChem (Germany). The Milli-Q deionized water (18 Ω) was obtained from the Brand Millipore system Milli-Q (France). Fetal bovine serum (HyClone, USA), trypsin-EDTA (tr-EDTA), Alpha Minimum Essential Medium (Alpha MEM), Dulbecco's Modified Eagle Medium (DMEM), ~~Hanks' Balanced Salt Solution (HBSS)~~, phosphate buffer solution (PBS), potassium chloride, potassium hydroxide, and ethyl alcohol undenatured (95%) were obtained from Biolot (RF) and used in the study. FITC Annexin V Apoptosis Detection Kits (Cat. No. 556547) were obtained from BD Pharmingen.

2.2. Preparation and characterization of biomaterials

2.2.1. Preparation of titanium coatings for ion track-etched membranes

The TMs used in the study were developed at the Joint Institute for Nuclear Research (Dubna, RF). A Mitsubishi PET film was used to obtain 23 mm-thick fabricated TMs with a pore density of 2.4×10^8 cm^{-2} and characteristic pore diameters of 0.3 μm. The TM fabrication process is described in detail elsewhere [24]. The irradiation was done using a cyclotron with the use of swift heavy ions (Xe, Kr) to create latent ion tracks on a PET film. These latent ion tracks were subsequently etched in

NaOH (2 M) to produce the pores. The track-etched PET membranes were thereafter made conductive by using a magnetron sputtering technique to deposit thin films of titanium (Ti) on the membrane. Integrating the Ti-based cathode into the TM improved the adhesion between electrospun nanofibers and the TM substrate and subsequently promoted larger-scale electrospinning [17]. The metallization of the TM with Ti (TiTM) was used to prepare the TM as a cathode for use during electrospinning. Ti as the coating was used due to its good electrical conductivity, ease of production by magnetron sputtering, stability in water, and biological inertness. The Ti metallic coatings were deposited from a vertically mounted target, which sputtered 99.7% pure Ti from an argon gas atmosphere (99.99%) carried out in an industrial direct current (DC) planar magnetron sputtering vacuum unit for roll-to-roll deposition. Glow discharge air plasma was used to clean the samples before depositing the Ti coatings on top of the TM for about a minute to improve the thin film adhesion to the polymer surface [25].

2.2.2. Chitosan–Collagen electrospinning solution preparation

Chitosan (0.54 g), collagen (0.54 g), and polyethylene oxide (PEO; 0.12 g) were dissolved in 20 ml of a solution containing deionized water, 96% ethyl alcohol, 1 M acetic acid mixed in a volume ratio of 55/45/5 parts. The mixture was stirred for 12 h with a magnetic stirrer at 180 rpm until the components were completely dissolved. The control value of the obtained solution viscosity was 1806 mPa × s at a solution temperature of 23 °C.

2.2.3. Direct electrospun fibers on metalized TMs and stabilization biolayer

The procedure for electroforming of nanofibers was carried out as previously described [26], namely, the electroforming of a chitosan nanoframe on PET TM with Ti was performed using the electrospinning system NANON-01A (MECC Co., Ltd., Fukuoka, Japan). Several parameters were used for spraying the chitosan nanoframe: 1) voltage – 28 kV, 2) solution dosing rate of 1 ml/hour, 3) die size of 0.210 mm, 4) distance from the die to the electrode of 15 cm, 5) an angle between the die and the electrode of 90 °, 6) rotation speed of the drum collector of 50 rpm, 7) speed of the die movement along the axis X = 1 cm/s, and 8) amount of sprayed solution of 1 ml.

Thermal and chemical treatments were used to stabilize the biolayer. The thermal treatment of the samples was carried out in a drying cabinet at a temperature of 120 °C for 1 h (the sample was named TiTMCC-120 °C). Chemical crosslinking was performed in GA vapors in a vacuum drying cabinet. For this purpose, the samples were placed in a drying cabinet after which 10 ml of 25% solution of GA was introduced into an open container and then air was pumped out at a maximum vacuum of 3 × 10^{-3} mbar. The exposure duration was 24 h at 37 °C (the sample was named TiTMCC-GA).

2.2.4. Physicochemical and structural–mechanical characteristics of biomaterials

For morphological analysis of the surface, a Hitachi S-3400 N scanning electron microscope (Hitachi, Japan) with thermal emission was used, and scanning was carried out in the secondary electron mode with an accelerating voltage of 15 kV. The resulting images were processed using the Gatan Digital Micrograph software package. The evaluation of the films' mechanical properties was carried out using a Shimadzu Universal Testing Machines AGS-X series (Shimadzu).

The studied samples had a cross-section of 10 × 0.023 mm. The working segment was 40 mm. The elongation of materials at rupture and the tensile strength were evaluated. Elongation of the material at rupture was estimated by the length of stretching (mm) before reaching the breaking stress limit. The tensile strength (σ) was calculated as the ratio of breaking force to the sample cross-sectional area (mm^2):

$$\sigma = \frac{p}{s}$$

in which P is the breaking force (H), and S is the sample cross-
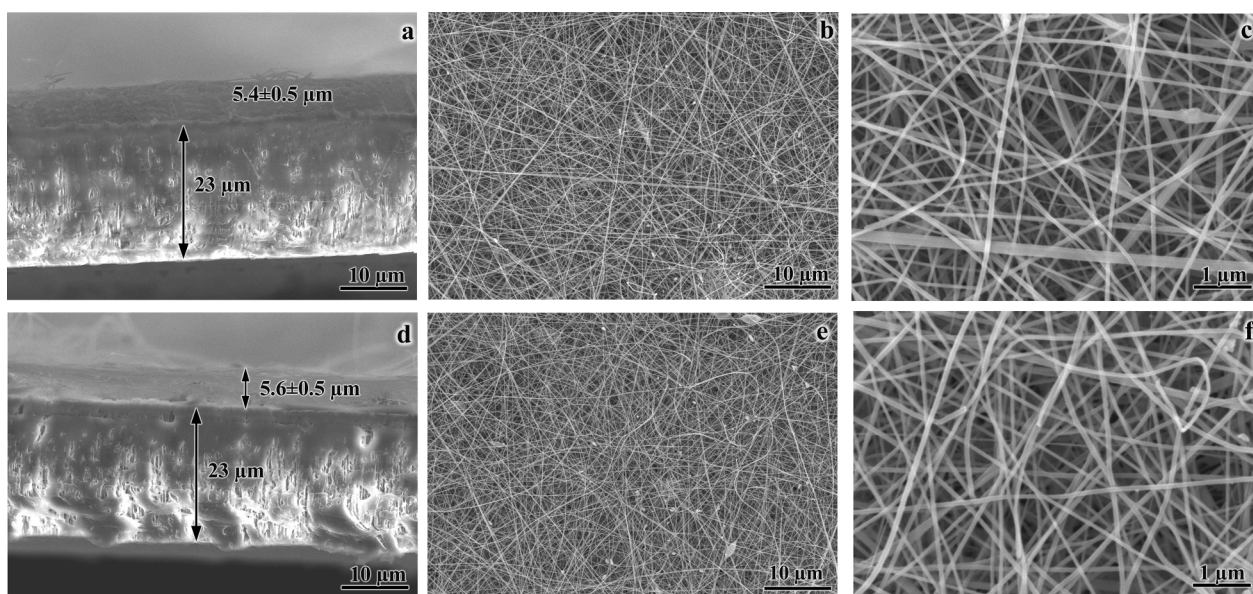
Fig. 1. Images of the profile (a1, b1) and the surface (a2, a3, b2, b3) of TiTMCC-120 °C (a1-3) and TiTMCC-GA (b1-3) biomaterials. The images were acquired using a Hitachi S-3400 N scanning electron microscope. Data are presented as means ± SD.

sectional area (mm^2).

Samples were placed in an electrokinetic cell using silver chloride electrodes to assess the electrokinetic potential of the flow (zeta potential). The method of measuring the flow potential (zeta potential) was obtained from [5]. A 0.01 M solution of potassium chloride (KCl) was used as the solution. To determine the recharge of the surface, KCl solutions with pH values = 3, 5, 7, and 9 were used. HCl and KOH solutions were used to set the pH value. The pressure of the solution ranged from 0.02 to 0.06 MPa in increments of 0.01 MPa. The measurements were performed in two modes. The step-by-step increase and decrease modes were used for setting the pressures of the solution. The value of the surface charge (zeta potential) was calculated using the Helmholtz–Smolukhovsky equation.

To determine gas and water permeability, biomaterial samples with diameters of 25 mm were used. The gas permeability of the samples was evaluated on the POROLUX 1000 capillary flow porometer (PORO-METER N.V., Belgium). The operating gas pressure ranged from 0.01 to 0.06 MPa in increments of 0.01 MPa. The water permeability of the samples was evaluated on a Millipore filtration cell stand in a dead-end mode at a deionized water pressure ranging from 0.02 to 0.06 MPa in increments of 0.01 MPa. All the studied samples were placed sideways with respect to the filtered water and contained a biolayer of applied chitosan and collagen.

2.2.5. Solubility estimation test

Stability against degradation *in vitro*.

The samples (d = 5 mm, n = 7) were placed in the wells of a 96-well plate and incubated with 0.3 ml PBS. The samples were incubated at 37 °C, and after 48 h, the samples were removed, weighed, and dried. The destruction of the biomaterial samples was evaluated using a scanning electron microscope based on the above-described method.

2.2.6. Cell adhesion to biomaterial

The adhesive properties of the studied biomaterials were assessed by the number of fibroblasts attached to the surface of the samples. To improve visualization of the cells, we performed preliminary staining of the cells with vital fluorescent dye PKH-26. Biomaterial samples (ø5 mm) sterilized with 70% alcohol treatment and ultraviolet (UV)-irradiation were placed into 96-well plates (one sample per well with five replicates) after which 0.1 ml of cell culture medium (Dulbecco's modified Eagle's medium [DMEM], 10% fetal bovine serum [FBS], 1%

penicillin–streptomycin [PS]) containing fibroblasts (5×10^4 cells/ml) was added to the wells. The number of replicates for each sample was seven. The incubation was performed under standard conditions (37 °C, 5% CO_2). After 6 h, the number and morphometric characteristics of fibroblasts were evaluated using both bright-field and fluorescence microscopy.

2.2.7. Cell proliferation

To assess the effects of the biomaterials on cell proliferation activity, co-incubation of the examined biomaterial samples with human fibroblasts was performed (Cell Applications, USA, Cat. No. 106 K-05a). To improve cell visualization, cells were pre-stained with vital fluorescent dye PKH-26. To characterize the proliferative activity, biomaterial samples (ø5 mm) were sterilized with 70% alcohol treatment and UV irradiation and then placed into wells of a 96-well plate, one sample per well with a total number of five replicates for each sample. An aliquot of 0.1 ml of cell culture medium (DMEM, 10% FBS, 1% PS) containing fibroblasts (2×10^4 cells/ml) were added to the wells. Culturing was performed under standard conditions (37 °C, 5% CO2).

At 24, 48, and 72 h after joint incubation of biomaterials with human fibroblasts, the number and morphometric characteristics of fibroblasts were evaluated. A Leica DMI4000 microscope (Leica Microsystems, Germany) and methods of bright-field, polarization, and fluorescent observation were used for morphometric characterization of cells. Cell proliferation evaluated by the number of cells per area 0.15 mm^2.

2.2.8. Measuring the number of apoptotic fibroblasts

Cell culture of human fibroblasts (Cell Applications, USA, Cat. № 106 K-05a) was introduced into the wells of a 12 well plate in the amount of 6–7×10^5/mL, after 1 h biomaterial samples (d = 10 mm, n = 7) were added to the cell suspension. Cultivation was carried out in 1 ml of cell culture medium (DMEM, 10% FBS, 1% PS), under standard conditions (37 °C, 5% CO2). A 72 h later, the culture medium and biomaterial samples was removed, adherent cells were separated using a tr-EDTA solution, after which the cells were washed three times in 10 ml of PBS, centrifuging for 5 min at 400g.

The FITC Annexin V Apoptosis Detection Kit (BD Pharmingen) was used to estimate the number of apoptotic cells. The procedure was carried out according to the manufacturer's protocol, namely, cells washed in PBS were resuspended in Binding buffer at a concentration of 1×10^6 cells/mL. 100 μL of the solution were transferred to 5 ml culture

Table 1
Mechanical properties of biomaterial.

Sample	Strength, Mpa	Elongation at break, μm
TiTM	28.60 ± 2,80	3.42 ± 0.10
TiTMCC-120 °C	29.07 ± 1,04	6.58 ± 0.10[a]
TiTMCC-GA	25.64 ± 1,31	8.13 ± 0.10[ab]

The data are presented as means ± SD. [a]– differences are significant compared to TiTM; [b]– differences are significant compared to TiTMCC-120 °C, at p < 0.05, n = 5.

tube; 5 μL of FITC Annexin V and 5 μL of Propidium Iodide were added. The cells were gently vortexed and incubated for 15 min at room temperature in the dark. 400 μL of Binding buffer were added to each tube and analyzed by flow cytometry (BD FACSCanto II) within 1 hr.

2.2.9. Hemolysis test

Human blood samples from healthy donors were collected in vacutainer tubes containing an anticoagulant. The samples were held for 2 h at room temperature followed by centrifugation at 350 g for 15 min at 48 °C. Subsequently, the red blood cells (RBC) were removed, washed four times in a 0.9% NaCl solution, and diluted 10-fold. The samples were placed in a 96-well plate, and 200 μL of RBC was added to each well and incubated for 1 h at 37 °C without stirring. The plate was then centrifuged (100 g, 5 min), and 100 μL from each well of the supernatant was collected from the wells. The optical density (OD) was measured at 540 nm using a microplate reader (iMark, BioRad). The positive control consisted of blood with distilled water (20 ml), while blood with a 0.9% NaCl solution (20 ml) served as the negative control. The level of hemolysis was calculated by the following equation [27]:

$$Hemolysis\ rate = \frac{OD\ sample - OD\ negative\ control}{OD\ positive\ control\ -\ OD\ negative\ control} \times 100\%$$

2.3. Statistical analysis

All experiments were performed at least in triplicate. The results are presented as means ± standard deviations (SD). Comparisons of data were made by using a two-tailed Student's *t*-test for independent data. The value of p < 0.05 was considered statistically significant.

3. Results and discussion

For this report, biomaterials, which are perforated PET-membranes with an electrically conductive layer of titanium (TiTM) on which a biolayer of a mixture of chitosan and collagen was applied by electroforming, were studied. The materials under study differed in terms of the method of stabilizing the biolayer; in one case, a thermal fixation method was used, and the sample was named TiTMCC-120 °C. In the other case, a chemical method with GA vapors was used (the sample was named TiTMCC-GA).

Morphological analysis of the biomaterial surface, which was carried out with a scanning electron microscope, demonstrated that the thicknesses of the ion-track membrane and the sprayed biolayer were 23 ± 0.01 and 5.5 ± 0.5 μm, respectively (Fig. 1). Spontaneously intertwined fibers with a thickness of 170 ± 40 nm formed the main structural element of the biolayer. A comparison of the obtained results with the literature data shows that such a surface structure is characteristic of all biomaterials obtained by electrospinning [28,29], including those formed on the TM surface [26].

The mechanical properties of the samples were evaluated by determining the rupture strength and elongation of the material under tension. It was shown that after spraying the bio-layer, the elongation of the membrane at rupture increased (Table 1). It was found that the elongation at rupture of TiTMCC-GA was 20% higher than that of TiTMCC-120 °C. At the same time, the tensile strength of TiTMCC-120 °C and TiTMCC-GA samples did not change and were comparable to TiTM
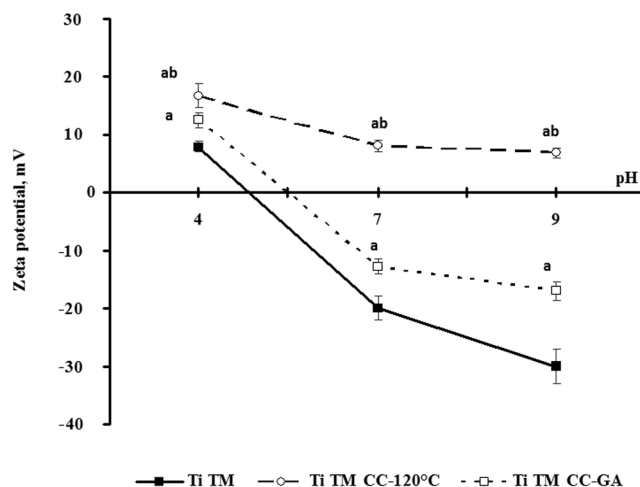
Fig. 2. The effect of acidity on the zeta potential of the surface of biomaterials. Data are presented as means ± SD. a – differences are significant compared to TiTM; b – differences are significant compared to TiTMCC-GA, at p < 0.05, n = 5.

without a sprayed bio-layer (Table 1).

The TiTMCC-120° and TiTMCC-GA biomaterials studied in this work differ from those manufactured earlier [5,26] due to the presence of collagen in their composition. As a rule, collagen is added to the composition of chitosan-containing biomaterials to increase biocompatibility and elasticity [30,31]. The results are consistent with data in the literature and show that the addition of collagen to the composition of chitosan and PEO fibers leads to an increase in the plasticity of the biomaterial by 40%.

Electrokinetic characteristics enable us to determine the isoelectric point and the charge sign of the biomaterial surface. It was found that in an acidic environment, all samples have a positive surface charge. Spraying of the bio-layer results in an increase in the zeta potential of the material surface, while the TiTMCC-120 °C charge was 40% higher than that of TiTMCC-GA (Fig. 2).

With an increase in the pH of the electrolyte, the surface charges of the samples decreased. The most significant changes in the zeta potential were observed for TiTM and TiTMCC-GA as at pH 9, the zeta potential of the surface of these materials decreased to − 32 and − 17 mV, respectively (Fig. 2). The TiTMCC-120 °C sample retained a positive zeta potential over the entire range of the electrolyte pH values used in this study (Fig. 2).

Thus, by applying one of several methods of stabilizing the biolayer on the surface of the ion-track membrane, it was possible to vary the charge of the biolayer surface. The regulation of the zeta potential of the surface was advantageous in terms of directed functionalization of the biomaterial. As methods of modifying the functional properties of the surface, the method of layer-by-layer self-assembly of polymers, variation of the structure, and ratio of polymers was used [32–34]. The use of chemical and thermal post-processing of electroformed polymers expands the list of biomaterial functionalization methods. At the same time, it should be noted that the difference in the potentials of the studied materials was about 50 mV, and it is not yet known how significant this difference is for manipulating the functional properties of the biomaterials.

Water and gas permeability were evaluated to characterize the capability of the biomaterial to provide water and gas exchange between the wound cavity and the environment. It was found that application of a bio-layer to the membrane causes a decrease in gas permeability and water permeability of the biomaterial by 20% and 50%, respectively (Fig. 3a, b). In addition, it was found that the permeability of the material was also affected by the method of biolayer fixation. For example, the water permeability of TiTMCC-120 °C was two times lower
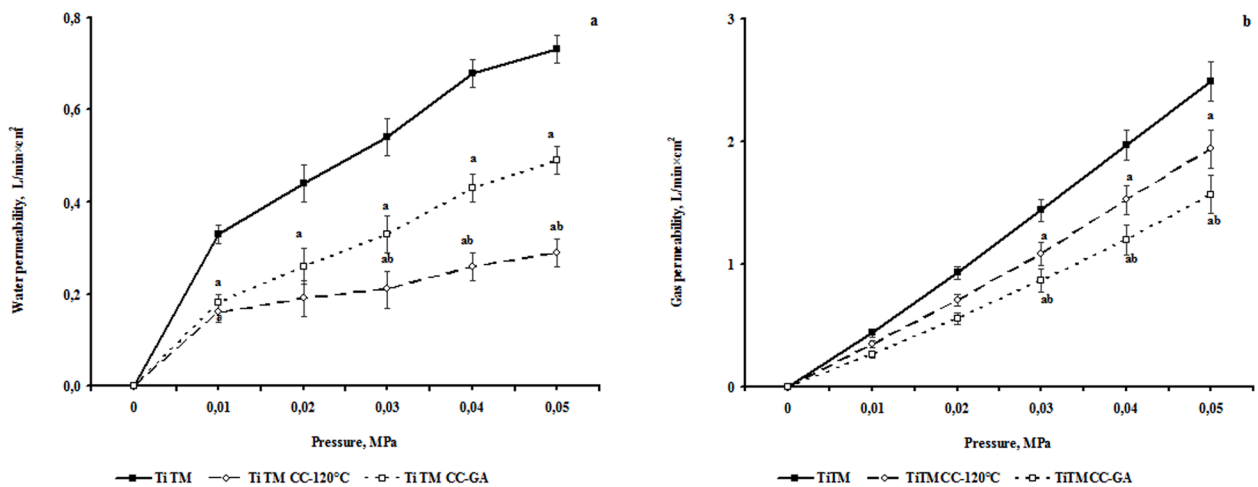
Fig. 3. Water (a) and gas (b) permeability of biomaterials. Data are presented as means ± SD. [a]– differences are significant compared to TiTM; [b]– differences are significant compared to TiTMCC-120 °C, at $p < 0.05$, $n = 7$.
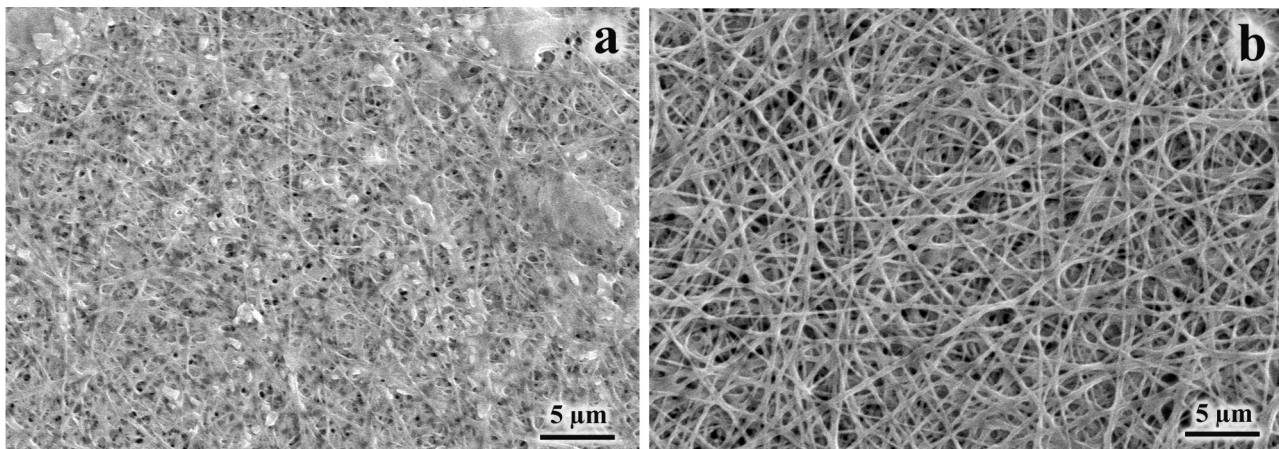
Fig. 4. Images of the surface of TiTMCC-120 °C (a) and TiTMCC-GA (b) biomaterials after 48 h of incubation in PBS. The images were taken using a Hitachi S-3400 N scanning electron microscope.
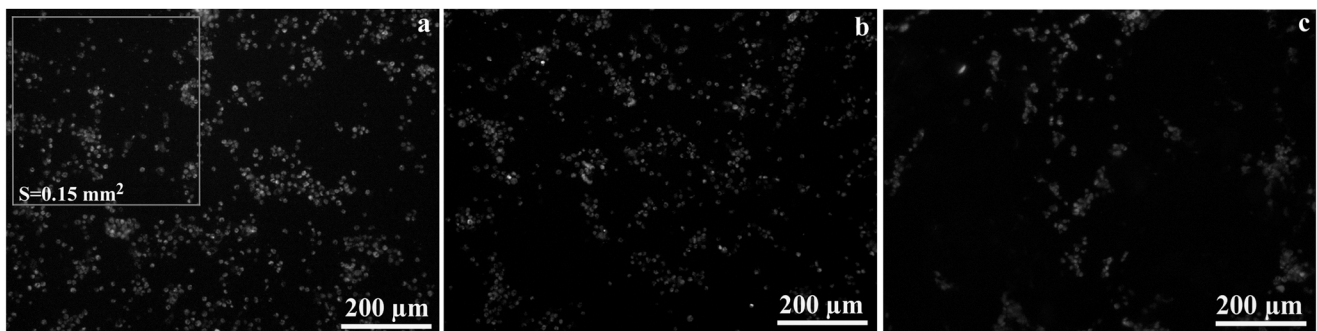
Fig. 5. Adhesion of fibroblasts on the TiTMCC-120 °C and TiTMCC-GA surface after 6 h co-incubation; a-control, b-TiTMCC-120 °C, c-TiTMCC-GA. Magnification × 50.

compared to TiTMCC-GA (Fig. 3a). At the same time, TiTMCC-120 °C showed high gas permeability (Fig. 3b).

The maintenance of optimal moisture content of the wound bed promotes tissue reparation, and the ability of the biomaterial to provide gas and moisture exchange is one of the requirements for modern wound dressings [35–37]. The obtained results demonstrate that the studied biomaterials can remove excess moisture from the wound cavity.

Analysis of images obtained using a scanning electron microscope

showed that the studied samples have different resistance to degradation in a PBS (Fig. 4). After PBS incubation the fibers of the TiTMCC-GA biolayer retained their shape, while the fibers of the TiTMCC-120 °C surface biolayer were not resistant to degradation in PBS.

At the next stage of the study, the biocompatibility of the samples was evaluated using cell adhesion, morphology, proliferation and viability of human fibroblast. Fibroblasts represent a heterogeneous cell population responsible for the production and remodeling of the dermal
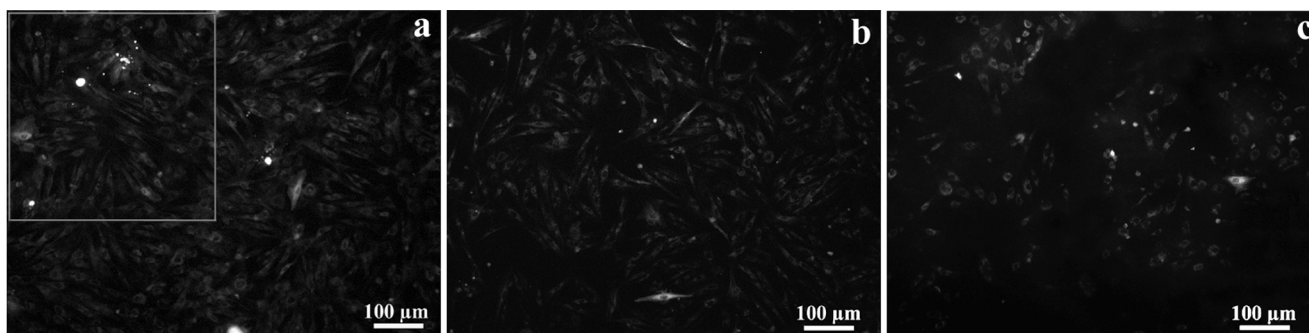
Fig. 6. Images of fibroblasts 24 h after incubation on the TiTMCC-120 °C and TiTMCC-GA surfaces; a-control, b-TiTMCC-120 °C, c-TiTMCC-GA. Magnification × 200.
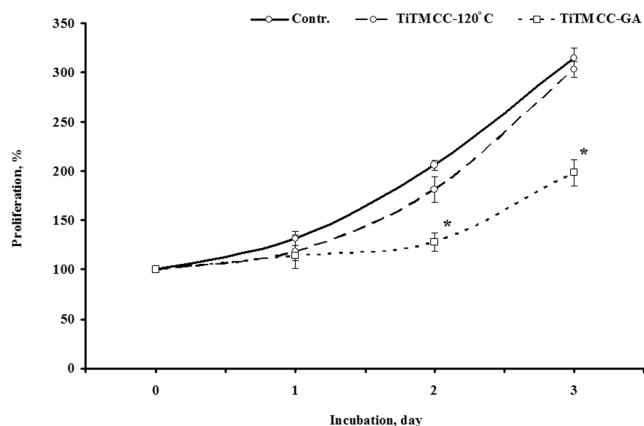
Fig. 7. Fibroblast growth curve during incubation with biomaterial samples. Data are presented as means ± standard deviation (SD). * – differences are significant compared to the control, when p < 0,05; n = 7.

Fig. 8. Effect of TiTMCC-120 °C and TiTMCC-GA on viability of fibroblasts after 72 h of co-incubation. Data are presented as means ± SD. * – differences are significant compared to the TiTMCC-120°, when p < 0,05; n = 7.

extracellular matrix. Fibroblast adhesion to the substrate plays an important role in many cellular processes, including cell migration and proliferation, as well as wound healing and angiogenesis [38–40].

After 6 h of incubation, 114 ± 27 cells adhered to the 0.15 mm^2 plastic surface (Fig. 5a). After 6 h of incubation, 98 ± 13 (Fig. 5b) and 57 ± 6 fibroblasts (Fig. 5c) were found to adhere to the same surface area of TiTMCC-120 °C and TiTMCC-GA samples, respectively. In both control wells and on the surface of the biomaterials, the cells were predominantly spherical in shape, with a surface area of 116 ± 17 μm^2 (Fig. 5a–c).

The cause of the decreased number of adherent cells on the surface of the TiTMCC-GA biomaterial is still not clearly understood. The studied biomaterials differed in terms of the zeta potential of the surface. At pH 7, the zeta potential of the TiTMCC-120 °C was + 10 mV, whereas the zeta potential of the TiTMCC-GA was –10 mV. It has been previously reported that adhesion of NIH-3 T3 fibroblasts [41] and osteoblasts [42] to biomaterials with higher surface potentials was higher than that to biomaterials with a negative potential. This finding appears to be due to the electrostatic attraction between the negatively charged cells and the positive surface. Possibly the bigger number of attached cells on the TiTMCC-120 °C surface is due to its positive potential. In addition, it cannot be excluded that the GA used to stabilize the biolayer in the TiTMCC-GA samples has a toxic effect on fibroblasts, thereby reducing their adhesive qualities. Previously, the efficiency of using GA vapors to increase the cytocompatibility of biomaterials was reported [43].

At the next stage of the study, the effects of the biomaterial specimens on the morphology and proliferative activity of fibroblasts were assessed. After 24 h of fibroblast culturing, approximately 50–60 cells per 0.15 mm^2 on the well surface. More than 90% of the cells were spindle-shaped with a cell size of 116 ± 15 μm^2. By increasing the
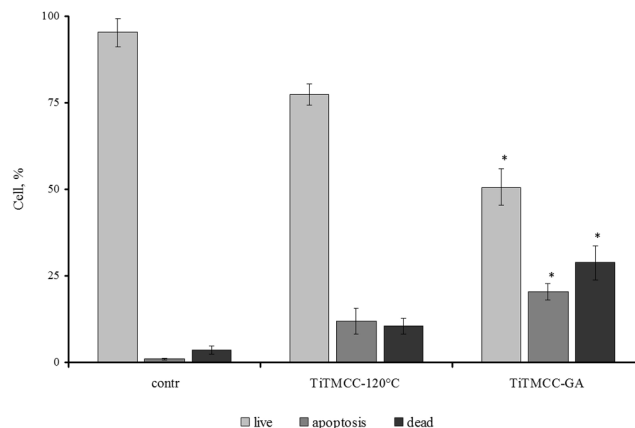
duration of cultivation, the number and size of cells increased. After 72 h, the number of cells increased more than threefold and was 115 ± 13 pcs/0.15 mm^2, and the cell body area reached 330 ± 59 mm^2 (Fig. 6a, Fig. 7). The data provided evidence of normal proliferative activity of the cell population.

It was shown that when fibroblasts were cultured on the surface of TiTMCC-120 °C samples, the morphometric characteristics of fibroblasts did not change and were comparable to the control values. For example, after 72 h of incubation, all cells were spindle-shaped, cell surface area was 340 ± 57 μm^2, and the number of cells per evaluated area was 95 ± 12 pcs (Fig. 6b). The proliferative activity is comparable to the control values (Fig. 7). TiTMCC-GA was found to inhibit fibroblast growth and proliferative activity, namely, by the end of the observation period, cells were predominantly globular in shape, body area was 94 ± 13 mm^2, and cell number per assessed area was 58 ± 6 pcs (Fig. 6c). The proliferative activity was reduced two-fold compared to control values (Fig. 7).

Assessment of the number of apoptotic cells showed that in controls, after 72 h, the number of live, apoptotic, and dead cells was $95\% \pm 4\%$, $1\% \pm 0.4\%$, and $4\% \pm 1\%$, respectively (Fig. 8). When fibroblasts were co-incubated with TiTMCC-120 °C, the number of live cells decreased to $77\% \pm 3\%$, and the number of apoptotic and dead cells increased to $12\% \pm 4\%$ and $11\% \pm 2\%$, respectively (Fig. 8). Co-incubation with TiTMCC-GA samples showed that the number of live cells was reduced by half, and the number of apoptotic and dead cells were $20\% \pm 2\%$ and $29\% \pm 5\%$, respectively (Fig. 8).

Hemocompatibility tests. During contact with red blood cells (RBC), certain materials can cause cell degradation and the release of hemoglobin. To test whether the material can cause hemolysis, hemolysis levels were evaluated by measuring the change in the optical density of the solution as a result of the release of hemoglobin from RBC after

Table 2
Hemolysis of red blood cells.

Sample	Optical density, 570 nm	Hemolysis, %
H_2O (positive control)	$2.17 \pm 0,29$	100
0.9% NaCl (negative control)	0.03 ± 0.01	1.5 ± 0.3
TiTM	0.06 ± 0.01	2.7 ± 0.4
TiTMCC-120 °C	0.05 ± 0.02	2.5 ± 0.7
TiTMCC-GA	$0.10 \pm 0.02^*$	$4.8 \pm 1.1^*$

The data are presented as means $\pm$ SD. *– differences are significant, at $p < 0.05$, n = 7.

membrane destruction. The levels of RBC hemolysis as a result of the interaction with biomaterials are shown in Table 2. The optical densities of the positive and negative controls were 2.17 and 0.03, which corresponds to 100 and 0% levels of hemolysis, respectively. The level of hemolysis during the interaction with biomaterials ranged from 2 to 5 %. These values are within the set range of the standard ISO 10993–4: 2017 [44]. The results showed that the developed TiTM, TiTMCC-120 °C, and TiTMCC-GA biomaterials did not cause visual damage to the RBC membranes during their contact. Therefore, these biomaterials can be considered hemocompatible.

Thus, in this study, we compared physicochemical, structural, and mechanical properties, in addition to biocompatibility of the TM with the applied biopolymer layer of chitosan and collagen after treatment of the biomaterial with GA vapor or a high temperature (120 °C). The main results of this study are described below:

1. The structure of the micro-relief of the electrospun biolayer on the surface of the studied TM does not depend on the method of stabilization.

2. Thermal treatment of biomaterials results in an increase in zeta potential of the surface of biomaterials.

3. Fixation of the biolayer with GA vapor led to a reduction in biocompatibility of the biomaterial by inhibiting the viability and proliferative activity of human fibroblasts *in vitro*.

4. Conclusion

Thus, it was found that the main structural elements of the TM surface covered with a biolayer of a mixture of collagen and chitosan are fibers. The coating of the ion-track membrane with a bio-layer preserves its gas and water permeability. The combination of the high biocompatibility of natural polymers and the stability of synthetic materials can be a successful strategy in manufacturing wound dressings of a new type with specified functional properties. Ion-track PET membrane with applied electrospun fibers from a mixture of chitosan and collagen can be used to produce the wound dressing.

Declaration of Competing Interest

The authors declare that they have no known competing financial interests or personal relationships that could have appeared to influence the work reported in this paper.

Data availability

The authors are unable or have chosen not to specify which data has been used.

References

[1] C. Lindholm, R. Searle, Wound management for the 21st century: combining effectiveness and efficiency, Int Wound J. 13 Suppl 2(Suppl 2) (2016) 5–15, https://doi.org/10.1111/iwj.12623.

[2] V. Jones, J.E. Grey, K.G. Harding, Wound dressings, Bmj. 332 (7544) (2006) 777–780, https://doi.org/10.1136/bmj.332.7544.777.

[3] K.C. Broussard, J.G. Powers, Wound Dressings: Selecting the Most Appropriate Type, American Journal of Clinical Dermatology. 14 (6) (2013) 449–459, https://doi.org/10.1007/s40257-013-0046-4.

[4] B. Hawthorne, J.K. Simmons, B. Stuart, R. Tung, D.S. Zamierowski, A.J. Mellott, Enhancing wound healing dressing development through interdisciplinary collaboration, J Biomed Mater Res B Appl Biomater. 109 (12) (2021) 1967–1985, https://doi.org/10.1002/jbm.b.34861.

[5] I.I. Vinogradov, L. Petrik, G.V. Serpionov, A.N. Nechaev, Composite Membrane Based on Track-Etched Membrane and Chitosan Nanoscaffold, Membranes and Membrane Technologies. 3 (6) (2021) 400–410, https://doi.org/10.1134/S2517751621060093.

[6] P. Apel, Track etching technique in membrane technology, Radiation Measurements. 34 (1) (2001) 559–566, https://doi.org/10.1016/S1350-4487(01)00228-1.

[7] A.B. Yeszhanov, I.V. Korolkov, S.S. Dosmagambetova, M.V. Zdorovets, O. Güven, Recent Progress in the Membrane Distillation and Impact of Track-Etched Membranes, Polymers (Basel) 13 (15) (2021), https://doi.org/10.3390/polym13152520.

[8] R.N. Carter, S.M. Casillo, A.R. Mazzocchi, J.S. DesOrmeaux, J.A. Roussie, T.R. Gaborski, Ultrathin transparent membranes for cellular barrier and co-culture models, Biofabrication. 9 (1) (2017), 015019, https://doi.org/10.1088/1758-5090/aa5ba7.

[9] J.H. George, D. Nagel, S. Waller, E. Hill, H.R. Parri, M.D. Coleman, Z. Cui, H. Ye, A closer look at neuron interaction with track-etched microporous membranes, Sci Rep. 8 (1) (2018) 15552, https://doi.org/10.1038/s41598-018-33710-6.

[10] K. Düregger, S. Trik, S. Leonhardt, M. Eblenkamp, Additive-manufactured microporous polymer membranes for biomedical in vitro applications, J Biomater Appl. 33 (1) (2018) 116–126, https://doi.org/10.1177/0885328218780460.

[11] C. Wang, S. Senapati, H.C. Chang, Liquid biopsy technologies based on membrane microfluidics: High-yield purification and selective quantification of biomarkers in nanocarriers, Electrophoresis. 41 (21–22) (2020) 1878–1892, https://doi.org/10.1002/elps.202000015.

[12] M. Katschnig, J. Wallner, T. Janics, C. Burgstaller, W. Zemann, C. Holzer, Biofunctional Glycol-Modified Polyethylene Terephthalate and Thermoplastic Polyurethane Implants by Extrusion-Based Additive Manufacturing for Medical 3D Maxillofacial Defect Reconstruction, Polymers (Basel) 12 (8) (2020), https://doi.org/10.3390/polym12081751.

[13] T.N. Nguyen, A. Rangel, D.W. Grainger, V. Migonney, Influence of spin finish on degradation, functionalization and long-term storage of polyethylene terephthalate fabrics dedicated to ligament prostheses, Sci Rep. 11 (1) (2021) 4258, https://doi.org/10.1038/s41598-021-83572-8.

[14] L. Al-Naamani, S. Dobretsov, J. Dutta, J.G. Burgess, Chitosan-zinc oxide nanocomposite coatings for the prevention of marine biofouling, Chemosphere. 168 (2017) 408–417, https://doi.org/10.1016/j.chemosphere.2016.10.033.

[15] R. Augustine, S.R.U. Rehman, R. Ahmed, A.A. Zahid, M. Sharifi, M. Falahati, A. Hasan, Electrospun chitosan membranes containing bioactive and therapeutic agents for enhanced wound healing, International Journal of Biological Macromolecules. 156 (2020) 153–170, https://doi.org/10.1016/j.ijbiomac.2020.03.207.

[16] A. Jafari, S. Hassanajili, N. Azarpira, K.M. Bagher, B. Geramizadeh, Development of thermal-crosslinkable chitosan/maleic terminated polyethylene glycol hydrogels for full thickness wound healing: In vitro and in vivo evaluation, European Polymer Journal. 118 (2019) 113–127, https://doi.org/10.1016/j.eurpolymj.2019.05.046.

[17] O.V. Artoshina, F.O. Milovich, A. Rossouw, B.L. Gorberg, L.D. Iskhakova, R.P. Ermakov, V.K. Semina, Y.K. Kochnev, A.N. Nechaev, P.Y. Apel, Structure and phase composition of thin TiO2 films grown on the surface of metallized track-etched polyethylene terephthalate membranes by reactive magnetron sputtering, Inorganic Materials. 52 (9) (2016) 945–954, https://doi.org/10.1134/s0020168516080021.

[18] I.R. Gilmutdinova, E. Kostromina, R.D. Yakupova, P.S. Eremin, Development of nanostructured bioplastic material for wound healing, Eur J Transl Myol. 31 (1) (2021), https://doi.org/10.4081/ejtm.2021.9388.

[19] C. Cui, S. Sun, S. Wu, S. Chen, J. Ma, F. Zhou, Electrospun chitosan nanofibers for wound healing application, Engineered Regeneration. 2 (2021) 82–90, https://doi.org/10.1016/j.engreg.2021.08.001.

[20] J. Xue, T. Wu, Y. Dai, Y. Xia, Electrospinning and Electrospun Nanofibers: Methods, Materials, and Applications, Chem Rev. 119 (8) (2019) 5298–5415, https://doi.org/10.1021/acs.chemrev.8b00593.

[21] C.A. Bode-Aluko, K. Laatikainen, O. Pereao, A. Nechaev, I. Kochnev, A. Rossouw, S. Dobretsov, C. Branger, A. Sarbu, L. Petrik, Fabrication and characterisation of novel nanofiltration polymeric membrane, Materials Today Communications. 20 (2019), 100580, https://doi.org/10.1016/j.mtcomm.2019.100580.

[22] P. Kianfar, A. Vitale, V.S. Dalle, R. Bongiovanni, Photo-crosslinking of chitosan/poly(ethylene oxide) electrospun nanofibers, Carbohydrate Polymers. 217 (2019) 144–151, https://doi.org/10.1016/j.carbpol.2019.04.062.

[23] M. Fadaie, E. Mirzaei, Z. Asvar, N. Azarpira, Stabilization of chitosan based electrospun nanofibers through a simple and safe method, Mater Sci Eng C Mater Biol Appl. 98 (2019) 369–380, https://doi.org/10.1016/j.msec.2018.12.133.

[24] P.Y. Apel, S.N. Dmitriev, Micro- and nanoporous materials produced using accelerated heavy ion beams, Advances in Natural Sciences: Nanoscience and Nanotechnology. 2 (1) (2011), 013002, https://doi.org/10.1088/2043-6262/2/1/013002.

[25] A. Rossouw, O.V. Artoshina, A.N. Nechaev, P.Y. Apel, L. Petrik, W.J. Perold, C. A. Pineda-Vargas, Stable Ion Beam Analysis (RBS and PIXE) Study of Photocatalytic Track-Etched Membranes, in: Exotic Nuclei, World Scientific, 2014, pp. 591–596.

[26] O. Pereao, C. Uche, P.S. Bublikov, C. Bode-Aluko, A. Rossouw, I.I. Vinogradov, A. N. Nechaev, B. Opeolu, L. Petrik, Chitosan/PEO nanofibers electrospun on metallized track-etched membranes: fabrication and characterization, Materials Today Chemistry. 20 (2021), 100416, https://doi.org/10.1016/j.mtchem.2020.100416.

[27] K.H. Seo, S.J. You, H.J. Chun, C. Kim, W.K. Lee, Y.M. Lim, Y.C. Nho, J.W. Jang, In vitro and in vivo biocompatibility of γ-ray crosslinked gelatin-poly (vinyl alcohol) hydrogels, Tissue Eng. Regen. Med. 6 (2009) 414–418.

[28] M. Zarei, A. Samimi, M. Khorram, M.M. Abdi, S.I. Golestaneh, Fabrication and characterization of conductive polypyrrole/chitosan/collagen electrospun nanofiber scaffold for tissue engineering application, International Journal of Biological Macromolecules. 168 (2021) 175–186, https://doi.org/10.1016/j.ijbiomac.2020.12.031.

[29] Schoeller J., Itel F., Wuertz-Kozak K., Gaiser S., Luisier N., Hegemann D., Ferguson S.J., Fortunato G., Rossi R.M. pH-Responsive Chitosan/Alginate Polyelectrolyte Complexes on Electrospun PLGA Nanofibers for Controlled Drug Release. *Nanomaterials*. 2021; 11(7): 1850. DOI: doi:10.3390/nano11071850.

[30] Z.G. Chen, P.W. Wang, B. Wei, X.M. Mo, F.Z. Cui, Electrospun collagen–chitosan nanofiber: A biomimetic extracellular matrix for endothelial cell and smooth muscle cell, Acta Biomaterialia. 6 (2) (2010) 372–382, https://doi.org/10.1016/j.actbio.2009.07.024.

[31] P. Wang, J. Liu, T. Zhang, <i>In Vitro</i> Biocompatibility of Electrospun Chitosan/Collagen Scaffold, Journal of Nanomaterials. 2013 (2013), 958172, https://doi.org/10.1155/2013/958172.

[32] M.S. Thomas, P.K.S. Pillai, M. Faria, N. Cordeiro, H. Barud, S. Thomas, L.A. Pothen, Electrospun polylactic acid-chitosan composite: a bio-based alternative for inorganic composites for advanced application, Journal of Materials Science: Materials in Medicine. 29 (9) (2018) 137, https://doi.org/10.1007/s10856-018-6146-1.

[33] H. Chen, J. Huang, J. Yu, S. Liu, P. Gu, Electrospun chitosan-graft-poly (ε-caprolactone)/poly (ε-caprolactone) cationic nanofibrous mats as potential scaffolds for skin tissue engineering, Int J Biol Macromol. 48 (1) (2011) 13–19, https://doi.org/10.1016/j.ijbiomac.2010.09.019.

[34] D. Li, F. Dai, H. Li, C. Wang, X. Shi, Y. Cheng, H. Deng, Chitosan and collagen layer-by-layer assembly modified oriented nanofibers and their biological properties, Carbohydrate Polymers. 254 (2021), 117438, https://doi.org/10.1016/j.carbpol.2020.117438.

[35] I.S. Kudryashova, P.A. Markov, E.Y. Kostromina, P.S. Eremin, A.P. Rachin, I. R. Gilmutdinova, Development of Wound Dressing for Regenerative Medicine, Bulletin of Rehabilitation Medicine. 20 (6) (2021) 84–95, https://doi.org/10.38025/2078-1962-2021-20-6-84-9.

[36] E.M. Tottoli, R. Dorati, I. Genta, E. Chiesa, S. Pisani, B. Conti, Skin Wound Healing Process and New Emerging Technologies for Skin Wound Care and Regeneration, Pharmaceutics. 12 (8) (2020), https://doi.org/10.3390/pharmaceutics12080735.

[37] R.L. Harries, D.C. Bosanquet, K.G. Harding, Wound bed preparation: TIME for an update, Int Wound J. 13 Suppl 3(Suppl 3) (2016) 8–14, https://doi.org/10.1111/iwj.12662.

[38] D. Avery, P. Govindaraju, M. Jacob, L. Todd, J. Monslow, E. Puré, Extracellular matrix directs phenotypic heterogeneity of activated fibroblasts, Matrix Biol. 67 (2018) 90–106, https://doi.org/10.1016/j.matbio.2017.12.003.

[39] D. Jiang, Y. Rinkevich, Scars or Regeneration?—Dermal Fibroblasts as Drivers of Diverse Skin Wound Responses, International Journal of Molecular Sciences. 21 (2) (2020) 617.

[40] K. Katoh, FAK-Dependent Cell Motility and Cell Elongation, Cells. 9 (1) (2020) 192.

[41] S. Metwally, S. Ferraris, S. Spriano, Z.J. Krysiak, Ł. Kaniuk, M.M. Marzec, S.K. Kim, P.K. Szewczyk, A. Gruszczyński, M. Wytrwal-Sarna, J.E. Karbowniczek, A. Bernasik, S. Kar-Narayan, U. Stachewicz, Surface potential and roughness controlled cell adhesion and collagen formation in electrospun PCL fibers for bone regeneration, Materials & Design. 194 (2020), 108915, https://doi.org/10.1016/j.matdes.2020.108915.

[42] L.-P. Xu, J. Meng, S. Zhang, X. Ma, S. Wang, Amplified effect of surface charge on cell adhesion by nanostructures, Nanoscale. 8 (25) (2016) 12540–12543, https://doi.org/10.1039/C6NR00649C.

[43] K.S. Rho, L. Jeong, G. Lee, B.-M. Seo, Y.J. Park, S.-D. Hong, S. Roh, J.J. Cho, W. H. Park, B.-M. Min, Electrospinning of collagen nanofibers: Effects on the behavior of normal human keratinocytes and early-stage wound healing, Biomaterials. 27 (8) (2006) 1452–1461, https://doi.org/10.1016/j.biomaterials.2005.08.004.

[44] *ISO 10993-4:2017. Biological evaluation of medical devices — Part 4: Selection of tests for interactions with blood (ISO Standard No. 10993-4:2017). Retrieved from https://www.iso.org/standard/63448.html.*